

EXPERIMENTAL ASSESSMENT OF MICROWAVE DIAGNOSTIC TOOL FOR ULTRA-WIDEBAND BREAST CANCER DETECTION

A. A. Bakar^{1,2,*}, D. Ireland¹, A. Abbosh¹, and Y. Wang¹

¹School of ITEE, The University of Queensland, St Lucia, QLD 4072, Brisbane, Australia

²Faculty of Electrical and Electronic Engineering, MARA University of Technology, Shah Alam, Malaysia

Abstract—An ultra-wideband microwave imaging system that employs a heterogeneous breast phantom and covers the ultra-wideband (UWB) frequency range (3.1 GHz to 10.6 GHz) is presented. The platform scanning system allows monostatic and bistatic mode of operation. In this work, developed heterogeneous phantoms are used to mimic the realistic breast tissues. A utilized tapered slot antenna array allows for a high resolution hemispherical scan, achieved by rotating the imaged object on a turntable. Full design details of the scanning system and the utilized post-processing algorithm are explained. To validate the reliability of the presented system, the results of several imaging cases, including the challenging low dielectric contrast case, are presented.

1. INTRODUCTION

At microwave frequencies, breast imaging methods have been explored for several decades. There are three different approaches to microwave imaging, namely the passive, hybrid and active methods. In the passive method, the tumor is detected based on the increase in its temperature compared to normal tissues. Hybrid methods use microwave energy to rapidly heat tumours and using ultrasound transducer to detect pressure waves generated by the elasticity properties of the heated tissues. Active methods involve illuminating the breast with microwaves and measuring the scattered signals.

Received 21 December 2011, Accepted 24 January 2012, Scheduled 30 January 2012

* Corresponding author: Aslina Abu Bakar (aslina@itee.uq.edu.au).

The use of microwave imaging for biomedical applications was initiated by Jacobi et al. in the late 70s. Antennas immersed in the water were designed to obtain images of internal structure of a canine kidney [1]. During the last decade, research activity in microwave imaging has mainly focused on the breast cancer detection.

In 2003, a medical model where microwave breast imaging is performed through a water-coupled boundary to detect breast cancer was developed by the school of engineering at Dartmouth College, USA [2]. In this experiment, modulated, continuous wave signals were transmitted from sixteen-monopole antennas operating over a frequency between 500 MHz to 3 GHz. Nine antennas at the other half of the imaging array (glycerin mixture) are used to receive the scattered signals. A superheterodyne technique is used to extract the phase and amplitude of the high frequency reflected signals. The reflected microwave signals are then converted into a 2D model map relating to the dielectric permittivity of breast tissues. However, the antenna array has to be moved manually via a hydraulic jack for the collection of multiple planar data required to get a model map of the breast tissues.

In 2009, Klemm et al. from the University of Bristol employed the UWB microwave radar using a real aperture array of UWB antennas that operate in a multi-static mode [3]. Antennas are positioned on a section of the hemi-sphere, conforming to the curved breast shape. The array is formed around the lower part of a 78 mm-radius sphere, in four rows of four antennas [4]. All antennas are aligned in rows and columns, and the array has two axes of symmetry.

In this paper, an automated high resolution hemispherical imaging system using ultra-wideband microwave signals is reported. The presented system enables a cylindrical scanning of a heterogeneous breast phantom. The main contribution of this paper is the integrated imaging system that includes a realistic breast phantom, directive antenna, and scanning platform. That system besides the presented imaging algorithm forms a complete diagnostic tool for breast cancer detection. To validate the reliability of the system, imaging results for three cases of early tumors are presented.

2. FABRICATION OF HETEROGENEOUS BREAST PHANTOMS

Homogenous phantoms have been of considerable use to test the principles of microwave imaging [5–7]. However, they are insufficient to test the feasibility of UWB imaging with respect to real breast tissues because of the composition of adipose and fibro glandular tissue [8].

Breast tissues heterogeneity is quite complex and different from one person to another. The phantom fabrication is not only motivated by the need for realistic breast phantom that can mimic the geometry and the dielectric properties of human breast, but also by the need for set of phantoms that can represent the range of human breast densities. Breast density is used to refer to the percentage of adipose and fibroglandular in the breast. In the developed phantom, it refers to the percentage of high dielectric material and low dielectric materials that represent adipose and fibroglandular, respectively.

The developed phantom emulates the dielectric properties of human breast over the UWB frequency range of 3.1 GHz to 10.6 GHz [9, 10] and covers a greater range of dielectric properties of normal tissue. Data published by Campbell and Land [11] reported on the high contrast between normal (fat and other tissue) and cancerous tissue. Another significant finding was that the heterogeneity and the complexity of the breast are higher than the previously reported. This is due to the almost random locations of the fat tissues with a low dielectric constant and the fibroglandular tissues with high dielectric constant. Heterogeneity of normal breast tissue has been underestimated by many early researchers [12, 13]. In 2007, a comprehensive study has suggested that the location of which the normal tissue samples were taken was the reason the heterogeneity was overlooked by previous studies [14]. The high dielectric constant of gland makes the contrast of normal tissues to cancerous tissues small, and thus, creates a challenge in the microwave detection methods.

The two breast phantoms used in our system, namely phantom A and phantom B, are fabricated to represent highly dense and low dense breasts as categorized in breast classification done on real breasts from reduction surgeries [15]. A low density breast is considered to have high fat content and low fibroglandular composition in the breast. Conversely, the high density breast has low fat content but high fibroglandular composition. In reality, the breasts of younger women contain less fat and are denser than older women's breasts. Thus, it is possible to assume that the developed phantom A represents breast of young women, whereas phantom B represents breast of older women. It is worth mentioning that a study [16] reveals that the risk of getting breast cancer increases with age.

Agar based material has been chosen in the fabrication of our phantoms since it can be easily shaped and has a stable dielectric properties over a long period of time. A pyrex glass mould is used to give a hemispherical shape to the phantoms. The hemispherical phantoms used in the experiment have a diameter of 13.4 cm. A random composition of fibroglandular mixture is deposited into the

base material of the breast phantom (fat tissue material) to simulate the heterogeneity [17]. By varying the composition of low dielectric materials such as cornflour and water, the dielectric properties of the phantom can be easily altered. In particular, the proposed phantom can represent varieties of women breasts from a low dense breast (dominance of adipose tissue), to a high dense breast (more heterogeneous mixture of fibro glandular and adipose). For the preparation of the tumor phantom, 7.68 g grape seed oil and 0.71 g detergent was mixed in a beaker. In a separate beaker, formaldehyde solution (0.313 g, 32%) and *p*-toluic acid were mixed by shaking with 3.14 g 1-propanol. 75 g milli-Q water was heated and the oil-detergent mixture was added. The formaldehyde and *p*-toluic acid mixture were then added together with 13.56 g of agar in small portions. 0.1 g alizarin dye was added to colour the tumor phantom which gives a red colour. The mixture was placed in suitable moulds and allowed to cool to room temperature [9].

The percentage of materials used in the developments of the two phantoms, in addition to the average and range of values for the dielectric constant, are shown in Table 1. Phantom A has a higher mean dielectric permittivity of 31.7 than phantom B that has a lower mean value of 28. The high volume percentage of agar mixture (high dielectric) with 60% composition and only 40% of corn flour mixture (low dielectric) making it have a high range of dielectric permittivity of 16.66 because the high concentration of dielectric constant of agar mixture which was randomly distributed in the phantom A. This value

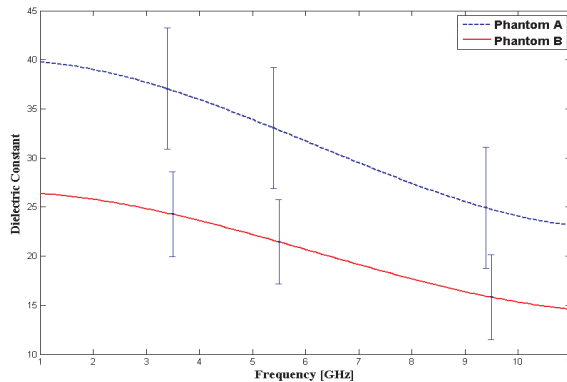


Figure 1. Measured dielectric constant of breast phantom samples for low and highly dense breast.

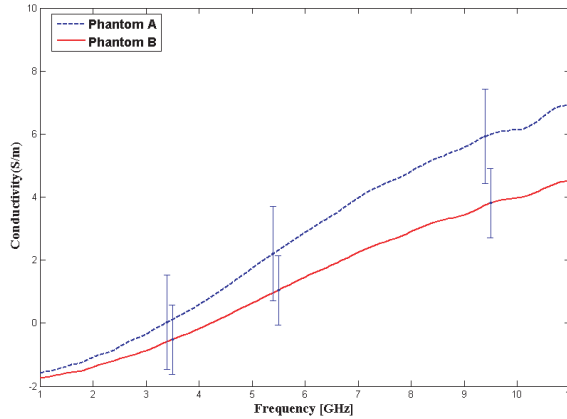


Figure 2. Measured conductivity of breast phantom samples for low and highly dense breast.

Table 1. The contents of phantoms (A and B), and mean and range of dielectric permittivity.

Phantom	% Volume of corn flour and water	% Volume of Agar mixture	Mean Dielectric Permittivity	Range of dielectric permittivity
A (Dense Breast)	60	40	31.7	16.66
B (Low Dense Breast)	80	20	28.0	11.72

confirms the high variability of the high density phantom A due to the extreme composition of low and high dielectric mixtures. The measured dielectric properties of the breast phantoms are depicted in Figure 1 and Figure 2. In this result, each of the curves with vertical bars represents the average dielectric properties of the breast phantom A and phantom B. The vertical bars also show the variability or the standard deviation of the measured dielectric properties of the phantoms from the average value. The heterogeneous hemispherical phantoms breast phantom used in the system has an average dielectric properties ($\epsilon = 18$ to 40 and $\sigma = 0.9$ to 7 S/m) to simulate normal breast tissues across the UWB frequency range. For the target (tumor), a mixture of agar, oil and formaldehyde solution is used with properties of ($\epsilon = 52$ and $\sigma = 1.8$ S/m).

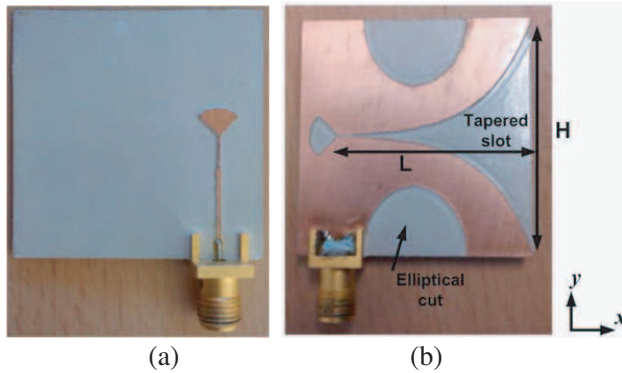


Figure 3. The bottom (a) and top (b) views of the tapered slot antenna.

3. SCANNING SYSTEM

3.1. Antenna

In the designed imaging system, a directive tapered slot antenna was used [18]. It is fed by a tapered microstrip-line with a suitable microstrip-slot transition. The slot is gradually tapered along the x -axis and symmetric along the y -axis towards the feed. The tapered slot is defined by an exponential function that is optimized for the best possible performance. The microstrip-slot transition, needed to achieve strong coupling between the microstrip feeder and tapered slot radiator, uses virtual open and short circuits in the form of a radial slot stub and a radial microstrip stub. From parametric simulations, it was found that by removing ellipse shaped regions from the conductive regions, the antenna produces a higher directivity in the lower part of the UWB [18]. The antenna is fabricated on Rogers RT6010LM substrate, featuring a dielectric constant of 10.2, a loss tangent of 0.0023, and thickness of 0.64 mm. The developed antenna (Figure 3) has a compact size of $36 \text{ mm} \times 36 \text{ mm}$. The optimum dimensions of the tapered slot for an ultra-wideband performance are found to be $H = 36 \text{ mm}$, and $L = 30 \text{ mm}$. As can be seen from Figure 4, the antenna operates from 3.1 GHz to over 10.6 GHz for the 10 dB return loss reference.

3.2. Scanning Platform

The scanning system configuration of the proposed UWB microwave imaging system is shown in Figure 5. The system uses a USB

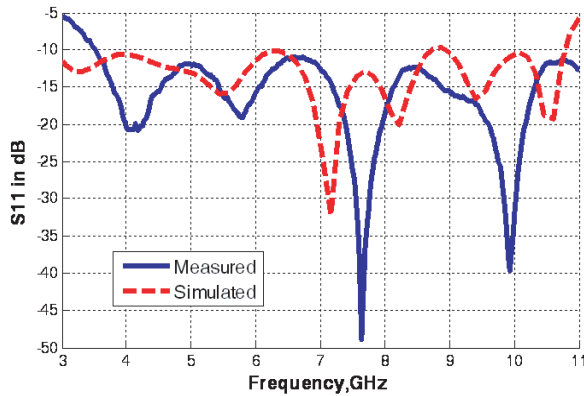


Figure 4. The reflection coefficient at the input port of the antenna.

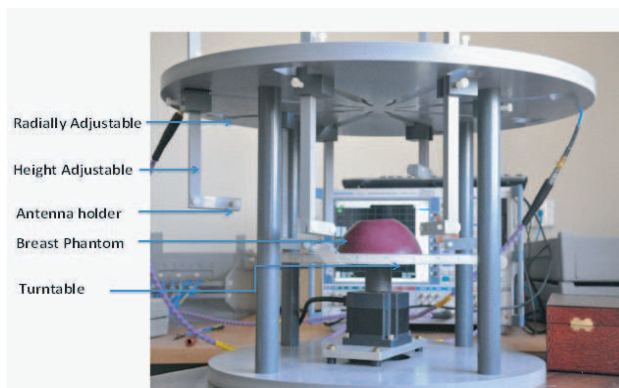


Figure 5. Scanning platform.

interface to activate a stepper motor to rotate the phantom at a minimal angular step of 0.72° . The developed system supports monostatic and bistatic mode of operation. In the work presented here, however, monostatic operation was used where a single antenna element is used for transmitting and receiving of the UWB pulses. The UWB pulses are generated using ZVA24 Rohde and Schwartz vector network analyser (VNA) in a step-frequency manner typically using 401 equidistant frequency points across the UWB. Obtaining the complex S -parameters is done using the virtual instrument software architecture (VISA). This is a standard for configuring and programming instrumentation via a variety of buses such as GPIB,

RS232, Ethernet and USB. The presented system employs a common Ethernet interface and requires less than 3 seconds to obtain 401 discrete complex numbers. In this system, a set of the ultra-wideband antenna elements depicted in Figure 3 can be offset from each other in the vertical and azimuth directions to minimize adverse effects of mutual coupling. Assuming that the array is limited to four antenna elements, ultra-wideband (UWB) data for image reconstruction can be acquired by antennas connected to a 4-port vector network analyser. To achieve a hemispherical scan, the imaged object is placed on the turntable (rotational axis) for a 360° scan while the elements of the array antenna are fixed and suitably spaced in vertical and azimuth directions. An adjustable antenna holder varies a radial position of the antenna from the phantom, depending on the size of the antenna and the phantom and also the antenna height.

4. RESULTS AND DISCUSSIONS

The designed system is used to image the fabricated heterogeneous phantoms. 50 antenna positions are considered with 7.2 angular steps. The antenna was placed at different horizontal planes. However, the best images that show the target clearly are obtained when the antenna is located at the same horizontal plane as the emulated tumor.

For the post-processing procedure needed to produce images and to quantify them, the algorithm and metric formulas proposed in [19] are adapted for this work. The underlying method of the algorithm is based on using transmitted ultra-wideband signals and recording of the time-domain back-scattered signals. This data has echo signals which ideally originated from electromagnetic scattering targets (e.g. breast tumor). The algorithm works by making a hypothesis that an echo signal originated from a given point; the normalized difference signals of each antenna are added at this space location. If the hypothesis for the particular scatterer location is correct, the signals add coherently and a large value of the sum is obtained. If the hypothesis is incorrect, the signals add incoherently and the sum is small. A continuous colour image is produced using a shading operator to interpolate at non-tested points. Strong intensity colours indicate the location of significant scattering objects.

Quantitative metrics are used to evaluate the produced image. In order to define the metrics used in this paper, it is necessary to first define several objects: p denotes any (x, y) point inside the body to be imaged (phantom); Z is the set of all discrete points; T is the set of (x, y) points that map to the location of the emulated tumor in the phantom. The function $I(p)$ gives the image intensity at point p . The

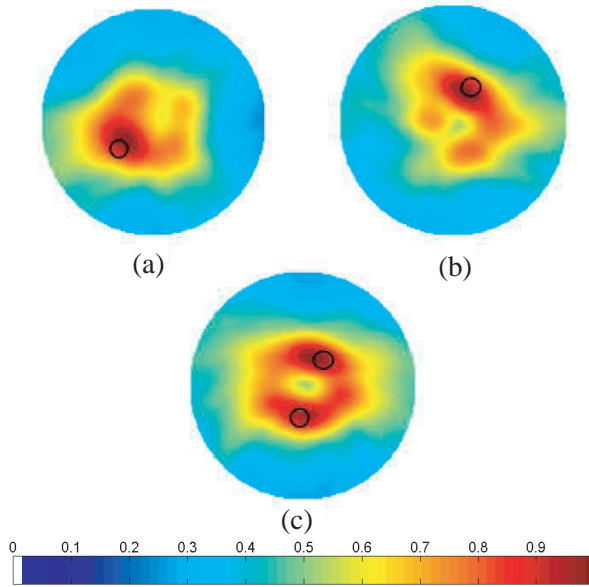


Figure 6. Imaging results of (a) Phantom A, (b) Phantom B, and (c) Phantom A with two targets inserted.

first metric used is the ratio of the average intensity value of points located in the tumor region over the other points located in normal breast tissue. It is given as

$$Q = \frac{\mu[I(p)] \quad \forall p \in \mathcal{T}}{\mu[I(p)] \quad \forall p \notin \mathcal{T}} \quad (1)$$

where $\mu[\cdot]$ denotes the mean function. A higher value for this metric implies the tumor intensity is more intensive than the background regions.

The second metric γ is the ratio of the maximum intensity value of the tumor region over the maximum intensity of the complete image [20]. It is given as

$$\gamma = \frac{\max[I(p)] \quad \forall p \in \mathcal{T}}{\max[I(p)] \quad \forall p \in \mathcal{Z}} \quad (2)$$

where the function $\max[\cdot]$ returns the maximum image intensity of the specified set of points. If this value is 1, it implies that the tumor is the strongest scatterer. If this value is less than 1, it quantifies the significance of the tumor in terms of electromagnetic scattering.

The above algorithm was used for post-processing. The imaging results of the phantoms are shown in Figure 6 for dense and low dense

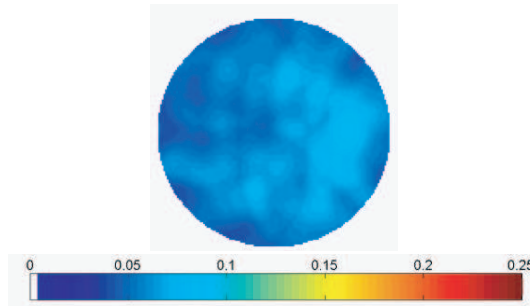


Figure 7. Imaging result when there is no target inserted.

phantoms. The low intensity color bar represents the low dielectric material (fat tissue), and high intensity color bar represents the high dielectric materials (fibro glandular and tumor tissue). The diameter of the target is 0.6 cm. The actual positions of the embedded targets in the utilized phantoms are indicated by the black circles in Figure 6. For phantom A with two targets, target T1 has 0.5 cm radius of a closed end cylinder filled up with water, whereas target T2 is the tumor fabricated material.

It is clear from the presented results in Figure 6 that the designed system as whole is able to detect small tumors even in a highly dense breast with a dielectric contrast as low as 1 : 1.3. The use of the system for the detection of two tumors in a dense breast was also successful as revealed in Figure 6(c) although there is a slight shift of a few millimeters in the central position of the detected targets in comparison with their actual positions. To verify that the system does not show false targets, the breast phantoms were imaged without an emulated tumor as shown in Figure 7 where no target can be seen.

To quantify the success of the imaging system, the metrics parameters are calculated for the imaging results. Table 2 shows the Q and γ metric results for the given images in Figure 6. Phantoms A and B show the image intensity at the tumor region was 1.9 and 2 times, respectively, more intense than the background intensity. The γ metric in both cases was 1 indicating the tumor was the strongest electromagnetic scatterer in both cases. For the phantom with two targets, which are denoted T_1 and T_2 as shown in Figure 6(c), the γ value was 1 for T_2 while T_1 was slightly lower at 0.96. This suggests that T_1 , consisting of water, is a slightly better electromagnetic scatterer than T_2 which consisted of material mimicking a tumor. Furthermore, the Q values for both targets were 1.795 and 1.73 respectively again showing the tumor intensity is at least 1.73 times higher than the background intensity.

Table 2. Performance of the algorithm for the phantoms with single and two targets.

Phantom		Q	γ
A		1.9	1
B		2	1
Two Targets	T_1	1.795	1
	T_2	1.73	0.96

5. CONCLUSION

This article reports the development of an ultra-wideband microwave imaging system using tapered slot antennas and heterogeneous breast phantoms aimed for breast cancer detection. The fabricated breast phantom closely mimics the realistic breast electrical properties and emulates the heterogeneity of real breast. Two classes of breast phantoms representing different breast density classifications are used in the imaging system. A reconstruction algorithm based on confocal imaging is used for post-processing. The obtained results indicate the possibility of detecting small tumors in situations with as low as 1 : 1.3 contrast in the dielectric constant. A future work will include the imaging of the phantom in 3D.

REFERENCES

1. Jacobi, J. H., L. E. Larsen, and C. T. Hast, "Water-immersed microwave antennas and their application to microwave interrogation of biological targets," *IEEE Transactions on Microwave Theory and Techniques*, Vol. 27, 70–78, 1979.
2. Meaney, P., S. Pendergrass, M. Fanning, and K. Paulsen, "Importance of using a reduced contrast coupling medium in 2D microwave breast imaging," *Journal of Electromagnetic Waves and Applications*, Vol. 17, No. 2, 333–355, 2003.
3. Klemm, M., I. J. Craddock, J. A. Leendertz, A. Preece, and R. Benjamin, "Radar-based breast cancer detection using a hemispherical antenna array — Experimental results," *IEEE Transactions on Antennas and Propagation*, Vol. 57, 1692–1704, 2009.
4. Klemm, M., I. Craddock, A. Preece, J. Leendertz, and R. Benjamin, "Evaluation of a hemi-spherical wideband antenna array for breast cancer imaging," *Radio Science*, Vol. 43, RS6S06, 2008.

5. Bindu, G., A. Lonappan, V. Thomas, C. K. Aanandan, and K. T. Mathew, "Dielectric studies of corn syrup for applications in microwave breast imaging," *Progress In Electromagnetics Research*, Vol. 59, 175–186, 2006.
6. Bindu, G., S. J. Abraham, A. Lonappan, V. Thomas, C. K. Aanandan, and K. Mathew, "Active microwave imaging for breast cancer detection," *Progress In Electromagnetics Research*, Vol. 58, 149–169, 2006.
7. Lazaro, A., D. Girbau, and R. Villarino, "Simulated and experimental investigation of microwave imaging using UWB," *Progress In Electromagnetics Research*, Vol. 94, 263–280, 2009.
8. Zastrow, E., S. K. Davis, M. Lazebnik, F. Kelcz, B. D. van Veen, and S. C. Hagness, "Development of anatomically realistic numerical breast phantoms with accurate dielectric properties for modeling microwave interactions with the human breast," *IEEE Transactions on Biomedical Engineering*, Vol. 55, 2792–2800, 2008.
9. Bakar, A. A., A. Abbosh, P. Sharpe, M. E. Bialkowski, and Y. Wang, "Heterogeneous breast phantom for ultra wideband microwave imaging," *Microwave and Optical Technology Letters*, Vol. 53, 1595–1598, 2011.
10. Bakar, A. A., A. Abbosh, P. Sharpe, and M. Bialkowski, "Artificial breast phantom for microwave imaging modality," *IEEE EMBS Conference on Biomedical Engineering and Sciences (IECBES)*, 385–388, 2010.
11. Campbell, A. and D. Land, "Dielectric properties of female human breast tissue measured in vitro at 3.2 GHz," *Physics in Medicine and Biology*, Vol. 37, 193, 1992.
12. Surowiec, A. J., S. S. Stuchly, J. R. Barr, and A. Swarup, "Dielectric properties of breast carcinoma and the surrounding tissues," *IEEE Transactions on Biomedical Engineering*, Vol. 35, 257–263, 1988.
13. William, Q. H. L., T. Joines, and G. Ybarra, *Electromagnetic Imaging of Biological Systems*, 2006.
14. Lazebnik, M., D. Popovic, L. McCartney, C. B. Watkins, M. J. Lindstrom, J. Harter, S. Sewall, T. Ogilvie, A. Magliocco, and T. M. Breslin, "A large-scale study of the ultrawideband microwave dielectric properties of normal, benign and malignant breast tissues obtained from cancer surgeries," *Physics in Medicine and Biology*, Vol. 52, 6093–6116, 2007.
15. Lazebnik, M., L. McCartney, D. Popovic, C. B. Watkins, M. J. Lindstrom, and J. Harter, "A large-scale study of the

- ultrawideband microwave dielectric properties of normal breast tissue obtained from reduction surgeries,” *Phys. Med. Biol.*, Vol. 52, 2007.
16. “SEER cancer statistics review,” U. Centers for Disease Control and Prevention Division of Cancer Prevention and Control, 1975–2007.
 17. Lai, J. C. Y., C. B. Soh, E. Gunawan, and K. S. Low, “Homogeneous and heterogeneous breast phantoms for ultra wideband microwave imaging applications,” *Progress In Electromagnetics Research*, Vol. 100, 397–415, 2010.
 18. Wang, Y., A. Bakar, and M. Bialkowski, “Reduced size UWB uniplanar tapered slot antennas without and with corrugations,” *Microwave and Optical Technology Letters*, Vol. 53, 830–836, 2011.
 19. Ireland, D. and M. E. Bialkowski, “Microwave head imaging for stroke detection,” *Progress In Electromagnetics Research M*, Vol. 21, 163–175, 2011.